Available online at www.sciencedirect.com
SCIENCE DIRECT®
Tectonophysics 372 (2003) 215–233
TECTONOPHYSICS
www.elsevier.com/locate/tecto

# Dislocation generation, slip systems, and dynamic recrystallization in experimentally deformed plagioclase single crystals

H. Stünitz[a,*], J.D. Fitz Gerald[b], J. Tullis[c]

[a] *Department of Earth Sciences, Istitut Geologisch-Palaontologisches, Basel University, Bernoullistr. 32, CH-4056 Basel, Switzerland*
[b] *Research School of Earth Sciences, Australian National University, Canberra, ACT 2601, Australia*
[c] *Department of Geological Sciences, Brown University, Providence, RI 02912, USA*

Received 4 February 2003; received in revised form 19 June 2003; accepted 23 June 2003

**Abstract**

Three samples of gem quality plagioclase crystals of An60 were experimentally deformed at 900 °C, 1 GPa confining pressure and strain rates of $7.5–8.7\times10^{-7}$ $s^{-1}$. The starting material is effectively dislocation-free so that all observed defects were introduced during the experiments. Two samples were shortened normal to one of the principal slip planes (010), corresponding to a "hard" orientation, and one sample was deformed with a Schmid factor of 0.45 for the principal slip system [001](010), corresponding to a "soft" orientation. Several slip systems were activated in the "soft" sample: dislocations of the [001](010) and ⟨110⟩(001) system are about equally abundant, whereas ⟨110⟩{111} and [101] in ($\bar{1}$31) to ($\bar{2}$42) are less common. In the "soft" sample plastic deformation is pervasive and deformation bands are abundant. In the "hard" samples the plastic deformation is concentrated in rims along the sample boundaries. Deformation bands and shear fractures are common. Twinning occurs in close association with fracturing, and the processes are clearly interrelated. Glissile dislocations of all observed slip systems are associated with fractures and deformation bands indicating that deformation bands and fractures are important sites of dislocation generation. Grain boundaries of tiny, defect-free grains in healed fracture zones have migrated subsequent to fracturing. These grains represent former fragments of the fracture process and may act as nuclei for new grains during dynamic recrystallization. Nucleation via small fragments can explain a non-host-controlled orientation of recrystallized grains in plagioclase and possibly in other silicate materials which have been plastically deformed near the semi-brittle to plastic transition.


*Keywords:* Dynamic recrystallization; Dislocations; Slip systems; Plagioclase deformation; Fracturing; Experimental deformation

## 1. Introduction

Despite the large data set of rock deformation experiments available, certain deformation processes are still poorly understood. In particular, the grain-scale processes associated with the brittle–plastic transition and the nucleation of grains during low temperature dynamic recrystallization remain poorly understood.

In the broad pressure–temperature region of the brittle–plastic transition, the progressive predominance of dislocation activity over fracturing processes with increasing temperature is well documented (e.g. Fredrich et al., 1989; Kohlstedt et al., 1995; Tullis and Yund, 1987, 1992; Hadizadeh and Tullis, 1992; Hirth

* Corresponding author. Tel.: +41-61-267-3596; fax: +41-61-267-3613.
*E-mail address:* holger.stuenitz@unibas.ch (H. Stünitz).

0040-1951/03/$ - see front matter © 2003 Elsevier B.V. All rights reserved.
doi:10.1016/S0040-1951(03)00241-5

and Tullis, 1994). However, the interaction of fracturing and dislocation activity is rather poorly documented (Wiederhorn, 1972; McLaren et al., 1989; FitzGerald et al., 1991; Hirth and Tullis, 1994; McLaren and Pryer, 2001) although fracturing may play an important role in the generation of dislocations and thus may facilitate the onset of crystal plastic deformation.

Progressive subgrain rotation is a well-established and effective way to generate new grains during dynamic recrystallization at moderate temperatures within the dislocation creep regime (Hobbs, 1968; Urai et al., 1986; Drury and Urai, 1990; Hirth and Tullis, 1992; Yund and Tullis, 1991). The nature of such a nucleation process implies that there is a systematic misorientation relationship between the host grain, the progressively rotated subgrains, and the recrystallized grains (host control). However, in many naturally deformed and dynamically recrystallized aggregates there is no host–control misorientation relationship between old and new grains (e.g. Ji and Mainprice, 1988, 1990; Kruse et al., 2001). Especially at low deformation temperatures where subgrains are absent and grain boundary bulging is dominant (regime 1 dislocation creep; Tullis and Yund, 1985; Hirth and Tullis, 1992; Gleason et al., 1993), the nucleation mechanism for new grains is not clear.

These two processes (the interaction of fracturing and dislocation activity and the nucleation of new grains during dynamic recrystallization) can best be studied in single crystal deformation experiments. Feldspar is well suited for such studies because in nature feldspar commonly fractures even during high temperature deformation (e.g. 600–800 °C) where dislocation creep is dominant (e.g. Goode, 1978; Sodre Borges and White, 1980; Brown and Macaudiere, 1984; Kruse and Stünitz, 1999; Kruse et al., 2001). Single crystal experiments on feldspar are also important because the relative importance of different slip systems in feldspar remains poorly known.

To study dislocation generation and interaction with other defects, it is necessary to use a dislocation-free sample material so that the generation of defects can be attributed exclusively to the experimental deformation. Some mafic volcanic rocks (e.g. from Hogarth Range, Australia, and Sonora, Mexico) contain porphyroblasts of plagioclase which have grown to considerable size at high temperatures in a magma and are dislocation-free. Because of the volcanic origin, these crystals have cooled to low temperatures very quickly so that they are only partially ordered. Ordering in intermediate plagioclase takes place at about 600–800 °C (Carpenter, 1994). Most plagioclase deformation experiments in the literature have been performed above 800 °C, so that deformation has been studied in the stability field of the disordered state. Using a starting material which is largely disordered has the advantage that dislocations are generated and can slip in their equilibrium disordered state at the high temperatures of the experimental conditions.

## 2. Results

### 2.1. Starting material

Deformation experiments were carried out on single crystals of labradorite from Sonora (Mexico). The gem-quality labradorite crystals (several centimeters in length) of composition An60 Ab38 Or2 are colourless to slightly yellow, and completely transparent. The composition of the labradorite crystals has been determined by quantitative EDS on a Cameca microprobe at 15 kV acceleration voltage (Table 1). The crystals are of volcanic origin from olivine basalts (Gutmann and Martin, 1976). The structural state has been determined using X-ray methods as a partially ordered C $\bar{1}$ plagioclase (Gutmann and Martin, 1976). In the transmission electron microscope (TEM), only very faint and diffuse satellite reflections are visible in the diffraction patterns. Some surfaces of the crystals are low

Table 1
Microprobe analysis (average of 18 analyses) of Sonoran labradorite starting material

| | wt.% | Atoms per 8 Oxygens |
|---|---|---|
| $SiO_2$ | 53.01 | 2.398 |
| $Al_2O_3$ | 29.83 | 1.590 |
| FeO | 0.36 | 0.013 |
| CaO | 12.49 | 0.605 |
| $Na_2O$ | 4.30 | 0.378 |
| $K_2O$ | 0.30 | 0.017 |
| Total | 100.29 | |
| | | An 60 |
| | | Ab 38 |
| | | Or 2 |

index crystallographic planes, mostly (100). The orientation of the crystals has been determined microscopically with a U-stage and macroscopically using the intersection of growth twins (mostly albite twins) with (100)-surfaces, combined with the habit of the grains (elongation in the [001]-direction).

No microfractures or dislocations have been observed in TEM foils of the starting material after inspection of several holes (Fig. 1), indicating a dislocation density of less than $10^8$ $m^{-2}$ (McLaren, 1991, p. 171). Thus, it can be concluded that the defects identified in deformed samples have all been introduced by the experimental deformation.

### 2.2. Deformation experiments

Samples of 6.35 mm diameter were cored from oriented Sonoran labradorite single crystals and the ends ground flat and plane-parallel. The sample length varied between 13 and 15 mm. Usually, single core pieces were too short, and two or three pieces of the same crystal orientation were stacked. Sample 1 had 0.1 wt.% $H_2O$ added between sample pieces, the others were deformed as-is (drying at 60 °C overnight after coring and grinding). All samples were placed in mechanically sealed Pt jackets inside a thin Ni-sleeve and deformed in a modified Griggs apparatus at 900 °C, 1 GPa confining pressure at strain rates of $7.5–8.7\times10^{-7}$ $s^{-1}$, to total strains of 8–10%, using an all-NaCl solid confining medium and end-pistons of $ZrO_2$. Samples 1 and 2 are oriented with their (010)-plane normal to the compression direction, sample 3 was oriented with the (010)-plane at 45° to the compression direction and the [001]-direction down-dip in (010). The direction of maximum compressive stress, $\sigma_1$, was normal to (021), resulting in a Schmid factor of 0.45 on the (010)[001] slip system (Table 2).

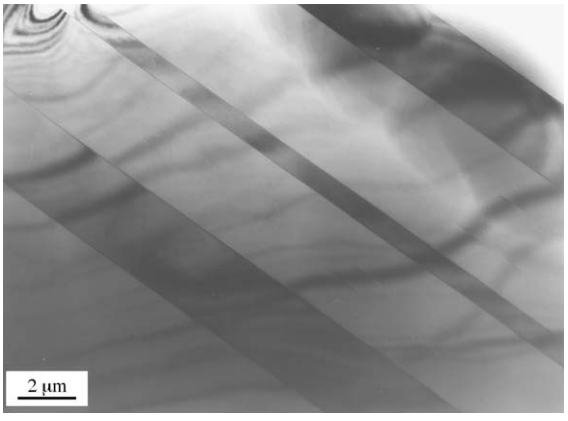


Fig. 1. TEM image of Sonoran labradorite starting material. Some albite growth twins are visible. No dislocations were detected in a scan of several holes in the foil, indicating a dislocation density of less than $10^8$ $m^{-2}$.

Table 2
Schmid factors in samples 1 and 2 ("hard orientation" = normal to (010)), and sample 3 ("soft orientation" = normal to (021)) for known plagioclase slip systems

| $b$ ($c$ = 7Å) | Slip plane 1 | Slip plane 2 | Slip plane 3 | Orientation |
|---|---|---|---|---|
| [001] | (010) M | (1$\bar{2}$0) MC | | |
| | 0.0 | 0.0 | | hard |
| | 0.448 | − 0.208 | | soft |
| [100] | (010) M | (001) MC | | |
| | 0.0 | 0.0 | | hard |
| | 0.0 | 0.0 | | soft |
| [101] | (010) MC + O | (11$\bar{1}$) MC | (13$\bar{1}$) MC | |
| | 0.0 | 0.0 | 0.0 | hard |
| | 0.391 | − 0.043 | 0.194 | soft |
| 1/2 [110] | (001) O | (1$\bar{1}\bar{1}$) O | | |
| | 0.060 | − 0.400 | | hard |
| | 0.422 | − 0.304 | | soft |
| 1/2 [1$\bar{1}$0] | (001) O | (11$\bar{1}$) O | | |
| | − 0.059 | − 0.351 | | hard |
| | − 0.419 | 0.046 | | soft |
| 1/2 [112] | (11$\bar{1}$) O | (20$\bar{1}$) MC | | |
| | 0.306 | − 0.002 | | hard |
| | − 0.080 | − 0.104 | | soft |
| 1/2 [1$\bar{1}$2] | (110) O | (20$\bar{1}$) MC | (021) M | |
| | − 0.354 | 0.002 | − 0.496 | hard |
| | 0.0 | 0.0 | 0.0 | soft |
| [102] | (20$\bar{1}$) MC + M | | | |
| | 0.0 | | | hard |
| | − 0.071 | | | soft |
| 1/2 [$\bar{1}$12] | (13$\bar{1}$) MC | | | |
| | 0.466 | | | hard |
| | − 0.122 | | | soft |

MC = Marshall and McLaren (1977a,b,); M = Montardi and Mainprice (1987), O = Olsen and Kohlstedt (1984, 1985).

### 2.3. Mechanical data

All samples attain a more or less constant flow stress after approximately 5–6% strain (Fig. 2). The different levels of flow stress of the samples are in part related to the crystal orientation. The most important slip system in plagioclase is considered to be (010)[001] (Marshall and McLaren, 1977a,b; Olsen and Kohlstedt, 1984, 1985; Montardi and Mainprice, 1987; Kruhl, 1987a,b; Ji and Mainprice, 1987, 1988, 1990), so that the orientation of sample nos. 1 and 2 represents a "hard" orientation because there is no resolved shear stress on this slip system. Indeed, sample nos. 1 and 2 show the highest peak flow stresses of about 800 and 500 MPa (Fig. 2). Sample 3 was oriented for near-maximum resolved shear stress on the (010)[001] slip system (Schmid factor = 0.45) and shows the lowest peak flow stress of about 300 MPa (Fig. 2).

The effect of added $H_2O$ appears to be contrary to what is expected because the $H_2O$-added sample (sample 1) in the "hard" orientation is stronger (by about 300 MPa) than the as-is sample (sample 2) in the same orientation (Fig. 2). However, the lower strength of the as-is sample probably reflects the larger proportion of deformed material within that sample compared to the water added sample 1 (approximately 40% more deformed material, measured along the length of the samples, Fig. 3). The larger volume of deformed material effectively implies a lower strain rate in the deforming regions of sample 2 than that in sample 1 and thus a lower flow stress.

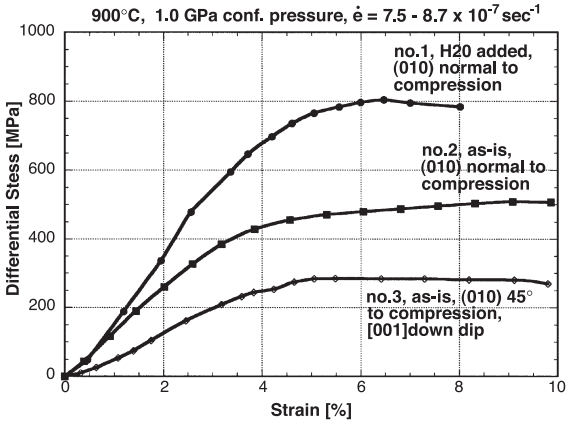


Fig. 2. Stress–strain curves for single crystal experiments of Sonoran labradorite. Samples 1 and 2 are oriented with the (010)-plane normal to the compression direction, sample 3 is oriented with the (010) plane at 45° and the [001]-direction down dip in (010). Sample 1 has had water added (0.1 wt.%), and the others were deformed as-is.

### 2.4. Microstructures

Plastic deformation in samples 1 and 2 (hard orientation for the (010)[001] slip system) is localized in rims at the contact surfaces between sample pieces and at the outer surfaces of the sample cylinders (Figs. 3 and 4a,b). Deformed rims are approximately 0.6–1.0 mm wide and are characterized by undulatory extinction, microfractures, and deformation bands (Fig. 4a). In contrast, deformation is more distributed throughout sample 3, although it is still heterogeneous.

In each section, the microstructural features will be described first for the hard orientation samples, then for the soft orientation sample, where both types of samples are concerned.

#### 2.4.1. Twinning

There are only few growth twins in the starting material—Fig. 1 is from an unusually twinned region. Therefore, most twins present in deformed samples 1 and 2 are deformation twins. They are recognized by a tapered shape and close association with fractures and deformation bands (Fig. 4c,d). Using the tapering sense as an indicator for twin propagation direction, it can be seen that all twins either extend from fractures (Fig. 4c) or terminate at deformation bands and fractures (Fig. 4c,d). In TEM, many of the tapered twins associated with microfractures and cracks have a length below 1 μm. All deformation twins follow the Albite twin law and have developed dominantly to one side of shear fractures (e.g. bottom part of sample 2, Fig. 3) or mainly on one side (in our case the $\sigma_1$ side) of conjugate shear fractures (Fig. 4c, only one set of conjugate fractures is shown). The (010) twin plane in samples 1 and 2 is normal to the compression direction and had no resolved shear stress acting on it. Thus, twinning is not a direct response to compression. As interpreted by McLaren and Pryer (2001) from similar microstructures, the twinning indicates stress relaxation around shear

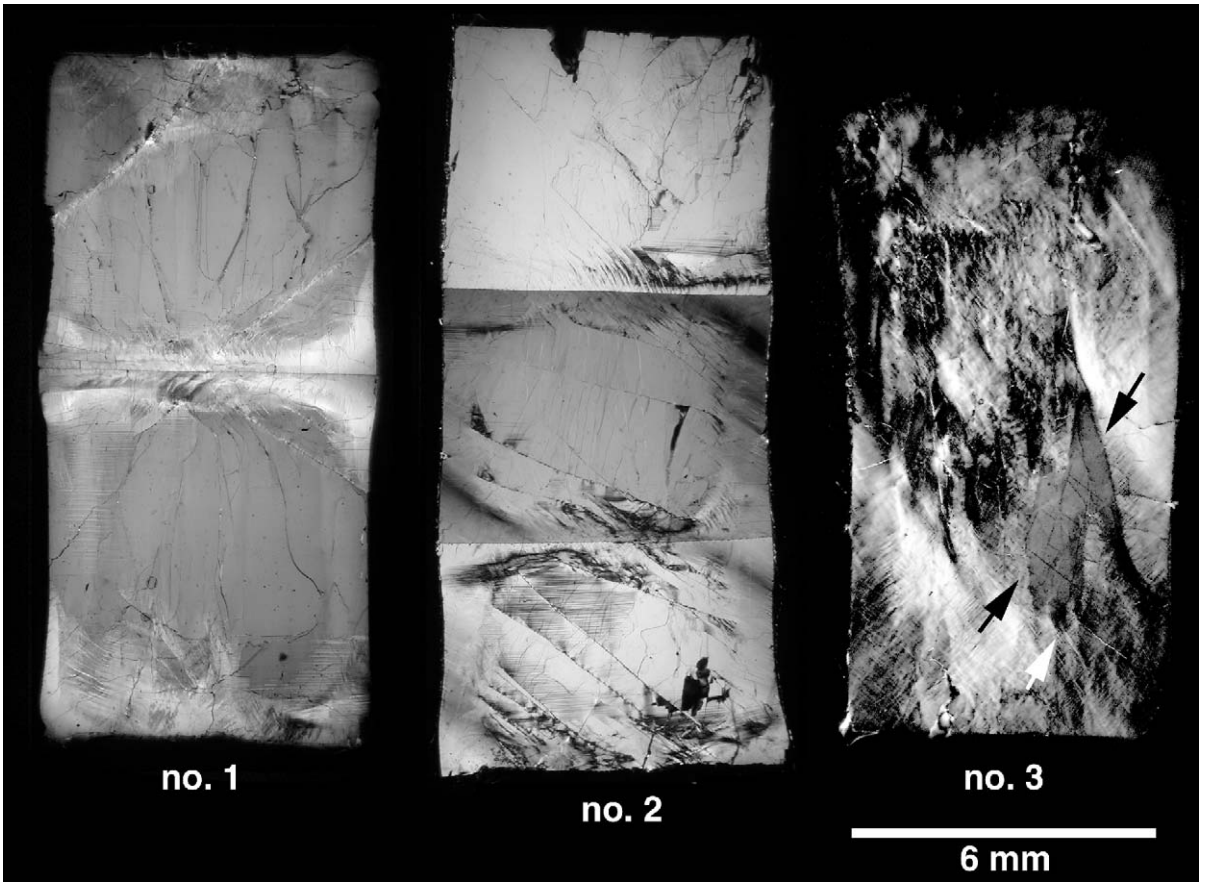


Fig. 3. Light micrographs (crossed polarizers) of the three deformed samples. Samples 1 and 2 consist of two and three pieces, respectively, and sample 3 of a single piece. Deformation in samples 1 and 2 is concentrated in the boundary region of the stacked cylinders and at the ends of the samples. In sample 3 most of the sample is pervasively deformed except for the small region between black arrows. The region at the tip of the white arrow is enlarged in Fig. 4g. None of the fine planar features in sample 3 are twins, they are all thin deformation bands. Compression direction is vertical in all samples.

fractures. As the Albite twinning could only operate in one shear sense in any crystal, an asymmetric distribution of twins developed with respect to the shear fractures in samples 1 and 2 (Fig. 4c). There is no difference in the extent or distribution of twinning between samples 1 and 2 and thus no apparent effect of water content on twinning.

Sample 3 does not show any twinning (Fig. 3) even though the orientation of the principal stresses corresponded to a high Schmid factor of 0.496 for both Pericline and Albite twin laws. Careful analysis showed that the sense of imposed shear was actually opposite to that required for deformation twinning (Borg and Heard, 1970) in this specimen.

*2.4.2. Fractures*

Two types of fractures occur in the samples: extension (mode 1) and shear (mode 2) fractures. One set of extension fractures is parallel or sub-parallel to $\sigma_1$ and forms in all samples but not to the same extent as in the samples of Marshall and McLaren (1977a,b), probably due to the higher temperatures and lower strain rates of our experiments. Another set of extension fractures formed normal to $\sigma_1$ during unloading. The unloading fractures in samples 1 and 2 only occur in the rims of undulatory extinction and terminate at the boundary between the region of undulatory extinction and the central region of the undeformed crystal (Fig. 4e). This observation can be explained by permanent plastic

deformation in the rim regions of undulatory extinction, whereas the inner parts of the samples only deform elastically or by displacement along shear fractures. When the sample is unloaded at the end of the experiment, the inner parts relax elastically or undergo reverse displacement along the shear fractures, putting the plastically deformed specimen rims into tension and producing mode 1 fracturing normal to σ1.

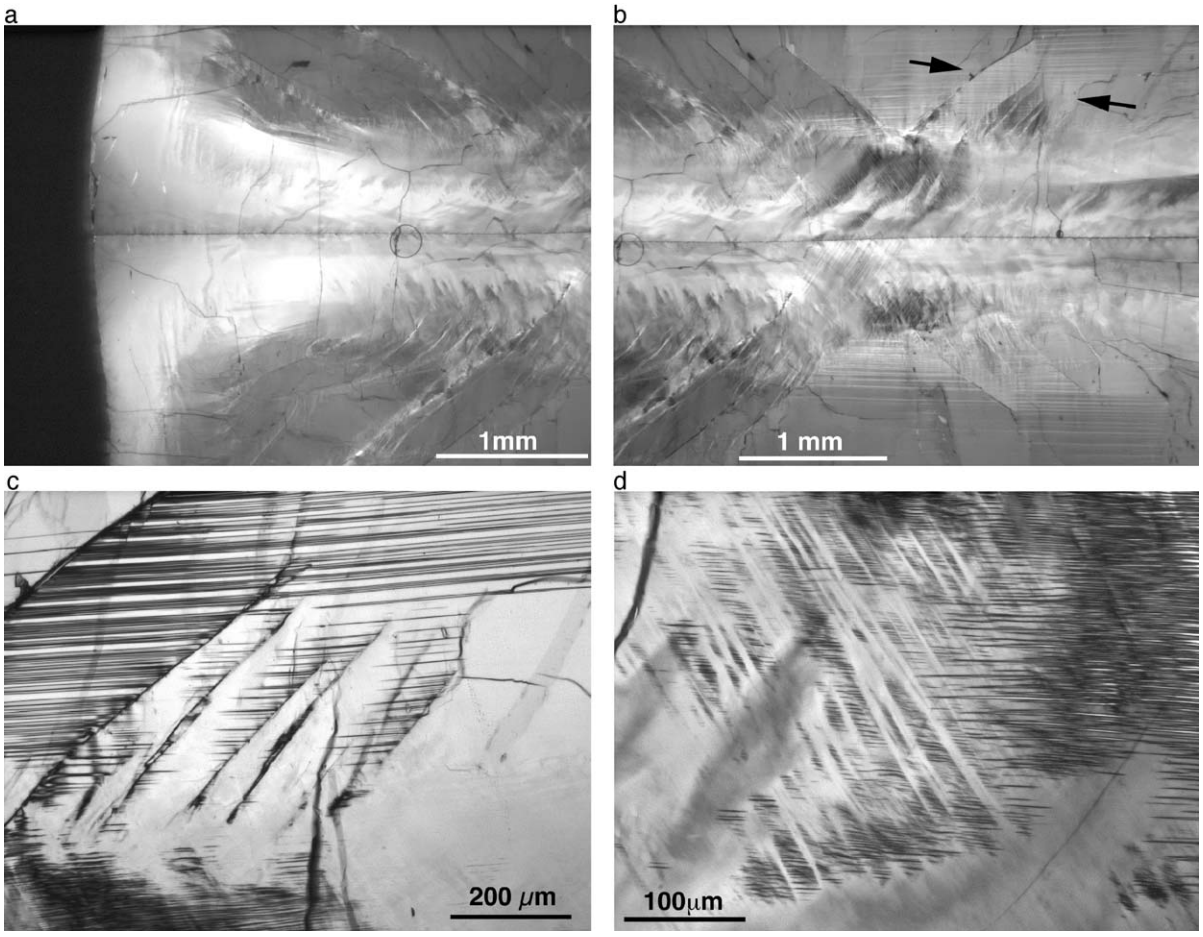


Fig. 4. Light micrographs of deformed samples. Shortening direction is vertical in all images except in (e), where it is horizontal. (a) Detail of the left margin of the central part of sample 1. The bulge shows the localized deformation of the sample. The light shade in the image marks a region at the margin of the sample pieces with different extinction angle (rim of undulatory extinction). The circle is a bubble resulting from thin section preparation. (b) Detail of the center part of sample 1. Conjugate shear fractures occur in the upper and lower sample piece and terminate at the rim of the region of undulatory extinction. The area between arrows is enlarged in (c). (c) Detail of albite deformation twins at one set of the conjugate shear fractures in the upper piece of sample 1 (for location see (b), region between arrows). Twins only form on the σ1 side of the conjugate shear fractures. (d) Detail of an area in the lower piece of sample 1. Albite deformation twins terminate at deformation bands. (e) Detail of the right hand rim of the center piece in sample 2 (compression direction horizontal). Extension (unloading) fractures (light in the image) only occur in the rim region of undulatory extension (lower part of the image). (f) Deformation bands in sample 1 (light in the image) extend with a SW–NE orientation from the termination (arrow) of a shear fracture, which is visible in the lower left hand quadrant of the image). The termination is located at the boundary of a region of undulatory extinction (upper half of the image), where there is almost no twinning visible. Twins are horizontal in the image. (g) Conjugate deformation bands in sample 3. The three medium grey regions in the upper part of the image correspond to the undeformed part of sample 3 (white arrow in Fig. 3) and contain no deformation bands and do not show undulatory extinction.

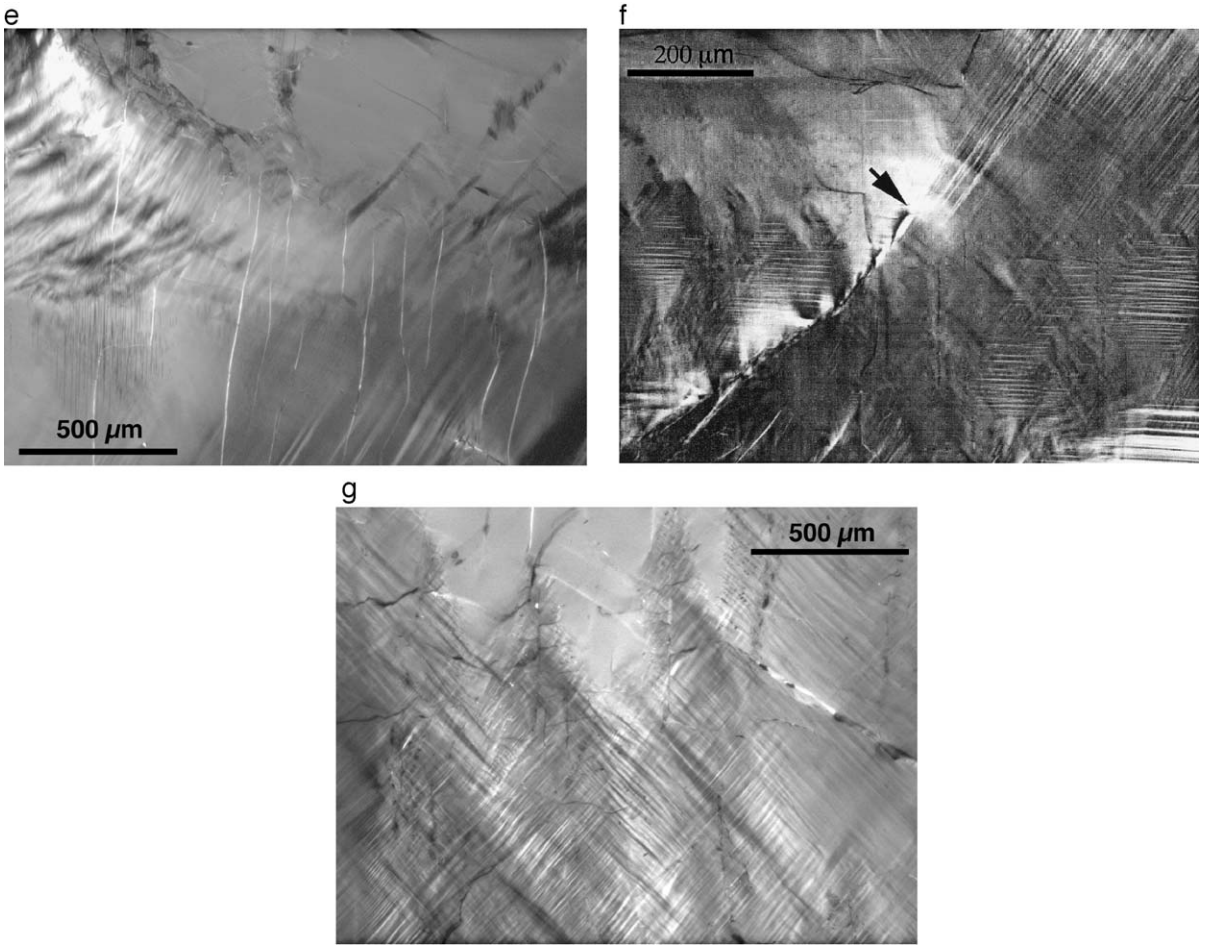


Fig. 4 (*continued*).

Thus, the extension fractures demonstrate that the zones of undulatory extinction indeed represent zones of crystal plastic deformation.

Most prominent shear fractures occur in samples 1 and 2 and only near the cylinder end surfaces in sample 3 (there are only few fractures in sample 3, and most of them are parallel to the $\sigma_1$ direction). Shear fractures are oriented 45–60° to $\sigma_1$ (Fig. 3). In some cases, conjugate sets of shear fractures develop (Fig. 4b). The shear fractures terminate at the plastically deformed rims of the sample pieces (Fig. 4f). In the TEM, shear fractures have an irregular but sharply defined boundary and consist of a narrow zone (approximately 1–2 μm wide, Fig. 5a) of crushed fragments. A high dislocation density occurs in the immediate vicinity of the fracture but the density diminishes within about 5 μm of the fracture. Adjacent to the shear fractures, there are straight arrangements of tangled dislocations and open pores indicating that the fracture process affected a zone around the fractures and that subsequently crack healing occurred (Fig. 5b, sample 3). Fragments inside the fractured zone range in size from ~ 0.1 to ~ 1 μm and display contrast of bent lattices (elastic strain) and/or dislocations. There are some very small grains (0.1 μm diameter) which have a rounded shape and are entirely defect-free (Fig. 5c). Such rounded shapes are unlikely to be produced by the fracture process but appear to result from some movement of grain boundaries during healing subsequent to fragmentation.

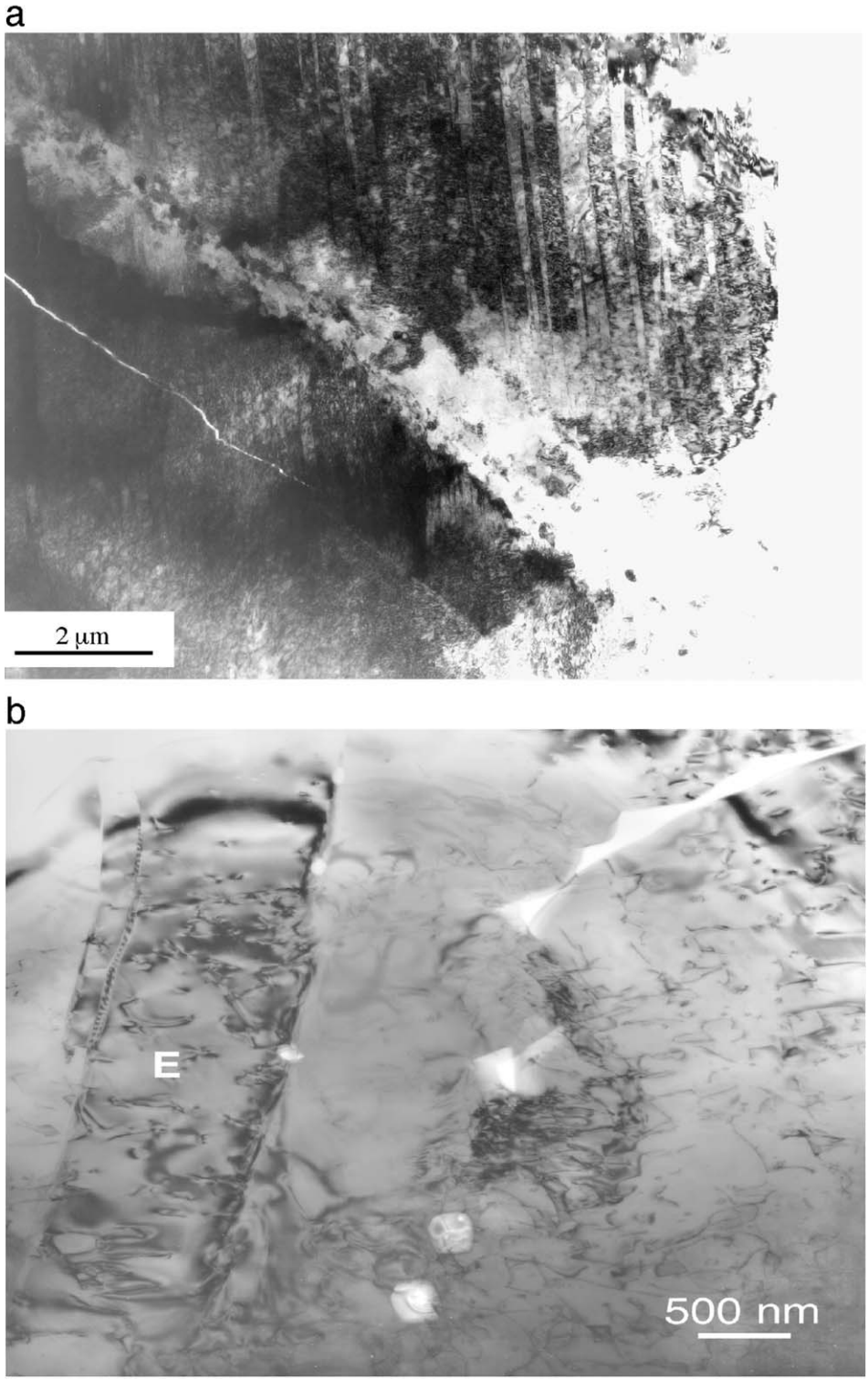
a
2 μm
b
E
500 nm

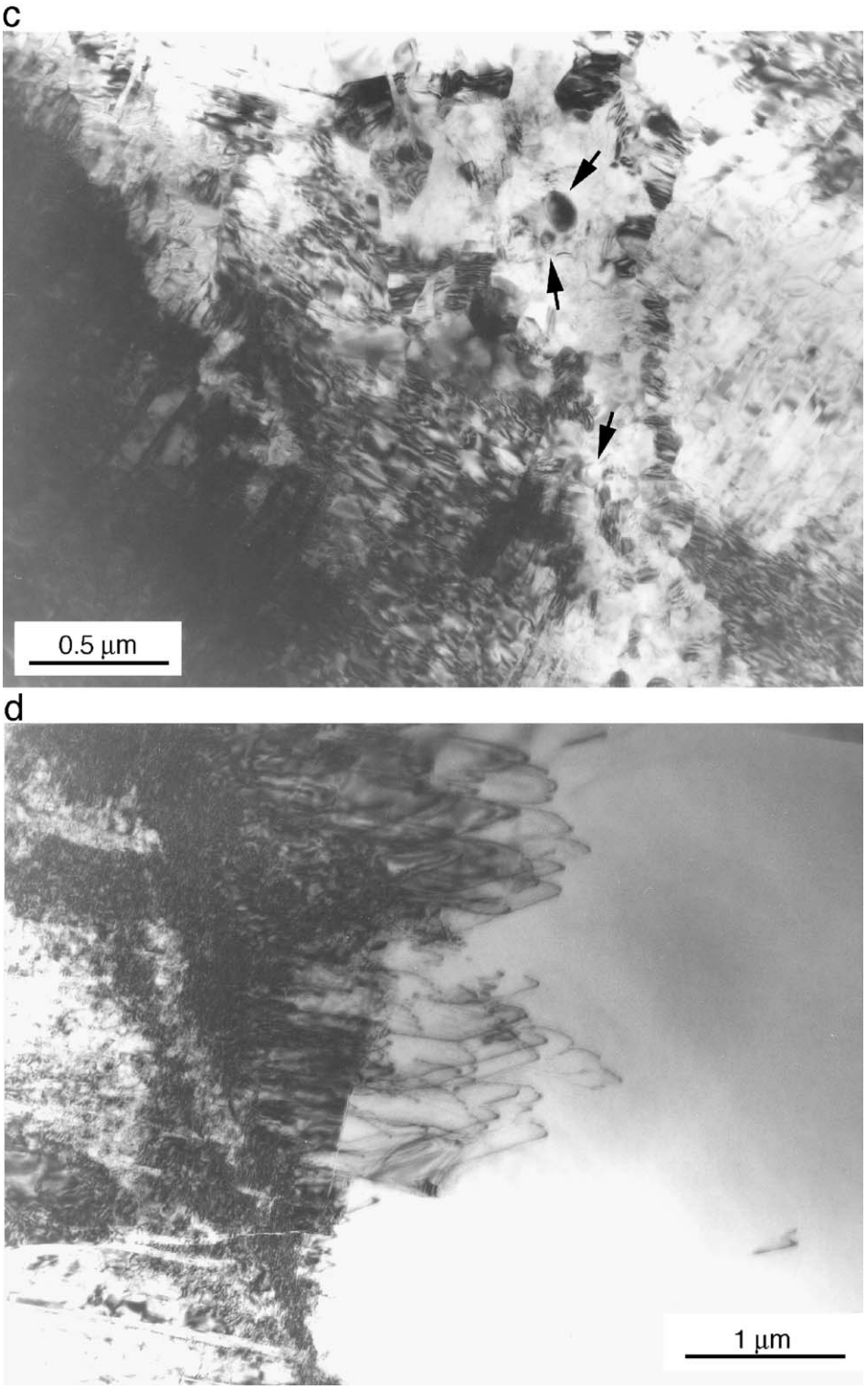


Fig. 5 (*continued*).

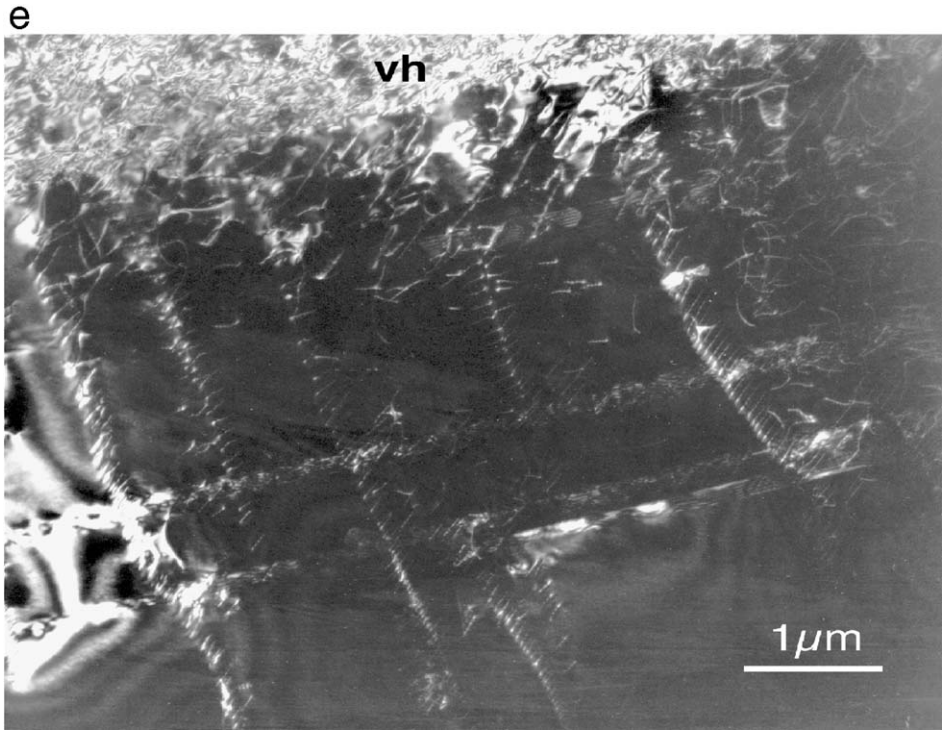


Fig. 5. TEM images of deformed samples. (a) A shear fracture in sample 1 (detail of fracture in Fig. 4f) runs ~ 45° to the compression direction, which is horizontal in the image (normal to the albite deformation twins). There is intense fragmentation of the grains in the fracture zone. In the immediate vicinity of the fracture the dislocation density is very high, decreasing over a short distance away from the fracture. The albite deformation twins are tapered and sometimes shorter than 1 μm. (b) An elongate dislocation cell (E) and adjacent open pore space are remnants of a healed fracture in the vicinity of a shear fracture (sample 3). (c) Detail of the crushed zone of shear fracture in (a). Fragments of variable size usually show high elastic strain or some dislocations. Some very small fragments are dislocation-free and have rounded shapes (arrows). (d) Detail of a deformation band in sample 1 (left part of TEM bright field image). The boundary of the band is sharp in most parts (e.g. at the bottom). Some glissile dislocations form loops and move away from the deformation band into the dislocation-free part of the crystal. (e) Arrays of dislocations with at least two different Burgers vectors spread out from sources in the region of very high dislocation density (a deformation band, VH) in sample 3.

*2.4.3. Deformation bands*

Shear fractures in the sample interiors do not penetrate the plastically deformed outer rims of the sample pieces. Where a shear fracture intersects a rim region, a set of very narrow parallel deformation features usually continues in the rim along the projection of the shear fracture (Fig. 4f). These deformation features will be termed deformation bands here. They resemble the ''deformation lamellae'' visible in the light microscope and described by Borg and Heard (1970). The deformation bands are elongated zones of high dislocation density (Fig. 5d), much like those described by Marshall and McLaren (1977a,b). In most cases, the bands are sharply defined but some glissile dislocations have moved away from the deformation bands into the defect-free crystal (Fig. 5d). The facts that twins terminate at the deformation bands (Fig. 4d) and also that tiny pores are associated with deformation bands suggest that many of these bands represent healed shear cracks (without visible offset and not containing fragments).

In sample 3 (''soft orientation''), the pervasively deformed portions of the sample (Fig. 3) are full of deformation bands, and many parts of the sample have two conjugate sets of deformation bands (Fig. 4g). There is no connection between deformation bands and shear fractures as the latter are almost absent in sample 3. Usually two sets of dislocations with different Burgers vectors (see below) have slipped away from the deformation bands (the regions of very

high dislocation density, Fig. 5e). The traces of the planes in which the dislocations slip correspond to those of the deformation bands. No twins or fragments have been observed within the deformation bands, even in those with the highest dislocation densities.

*2.4.4. Dislocations and slip systems*

Dislocations are only observed in regions that show undulatory extinction in the light microscope-regions with uniform extinction are dislocation-free in TEM. The transitions between regions with and without dislocations usually are sharp (one to a few microns wide; Fig. 5d,e). Slip systems have been determined in TEM using invisibility criteria in weak beam dark field (WBDF) images combined with slip trace analysis (Marshall and McLaren, 1977a,b). Due to the elastic anisotropy of feldspars, the observed contrast should ideally be compared with calculated images as has been done by Olsen and Kohlstedt (1984) and Montardi and Mainprice (1987). However, our analysis has been guided by known slip systems (Table 2) and has used only invisibility criteria (especially in WBDF images with high deviation from exact Bragg condition) and slip trace analysis.

In the "soft" sample 3 (Fig. 6), two almost orthogonal sets of dislocations are imaged. One set with mostly straight dislocations lies in the (010) plane (Fig. 6b). These are [001](010) dislocations (Table 2) making very elongated rectangular loops with long screw and short "edge" segments (true edge character is not possible in triclinic crystals), similar to what is described by Olsen and Kohlstedt (1984) and Montardi and Mainprice (1987). The other set of dislocations in sample 3 has a ⟨110⟩-type Burgers vector, and these have slipped in planes oriented from {111} to (001) (Table 2), probably (001) being the dominant slip plane. These two sets of dislocations can both be observed to originate from deformation bands (Fig. 5e). Another, less abundant, set of dislocations observed in sample 3 has Burgers vector [101], with screw segments that slipped on planes between $(\bar{1}31)$ and $(\bar{2}42)$. In sample 3, all of the observed slip systems have high Schmid factors (Table 2).

In the "hard" sample 1, dislocations with a ⟨110⟩ Burgers vector or [001](010) slip system have also been identified despite the fact that there was no resolved shear stress on the [001](010) slip system in this sample. No dislocations of the common slip systems with Burgers vector [100] have been observed in any of the samples, probably because there was no shear stress acting on these systems in either sample orientation (Table 2).

In samples 1 and 3, the different slip systems form sets of dislocations which do not show much interaction with each other; there are few pinned dislocations and jogs, and no densely tangled dislocations of the different sets. The observed planar arrays of dislocations are never simple tilt or twist boundaries. All observed arrays of dislocations appear to represent slip planes or possibly healed cracks. Some crack healing is indicated by sets of large pores as in Fig. 5b, but only a few of the dislocation arrays show any association with such porosity. No low angle subgrain boundaries have been observed, indicating that thermally activated recovery has not occurred.

*2.4.5. Double images of [001] dislocations*

Close examination of dislocations with [001] Burgers vector shows that all are characterized by a double image with splitting confined to the (010) plane (Fig. 7). Such image splitting in dark-field images is largest for dislocations with near-edge geometry and is usually 30–40 nm but can be up to 60 nm. Splitting is smallest for segments in screw orientation. The region lying between the two parts of each double image shows a weak fault-like contrast, best seen in (*hk*0) images where [001] dislocations are out of contrast. Strangely, no fault contrast can be observed using the strong reflection $g = 002$ when the dislocation visibility is very high (Fig. 7). In this condition, however, asymmetry is normally present in the doubled image with one of the pair being brighter than the other. This asymmetry can be reversed by choosing either reverse g or reverse s (deviation from Bragg condition). Unfortunately, detailed imaging experiments using weak-beam invisibility and the method of Ishida et al. (1980) have been inconclusive in identifying either Burgers or stacking-fault vectors. Whatever the nanometer-scale details of these dislocations, they appear to be very mobile and glide extensively in the (010) slip plane.

*2.4.6. Particles*

Some small particles (size < 20 nm) have been observed in deformed specimen 1, using the TEM, but not in the starting material. EDS analyses and

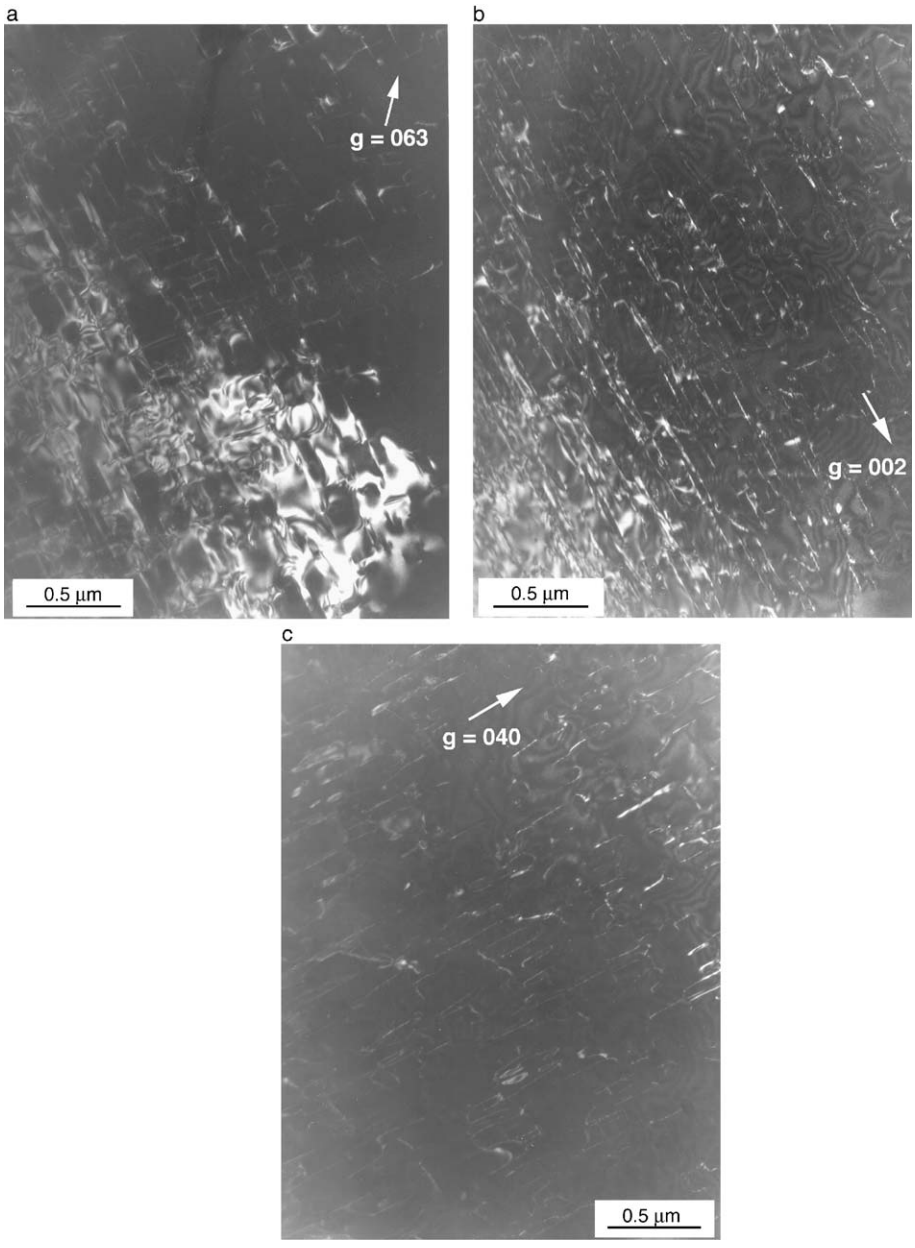


Fig. 6. TEM-Weak beam dark field (WBDF) images of dislocations (sample 1). (a) WBDF of two sets of dislocations visible with $g = 063$. (b) The same area as (a) taken with $g = 00\bar{2}$, and only one set of dislocations is visible. The slip system of the visible set is [001](010). The straight dislocations lie in the (010) plane. (c) The same area as (a) and (b) taken with $g = 040$, and only the other set of dislocations of (a) is visible. The slip system of the visible set of dislocations is ⟨110⟩(001). Many dislocations form loops in (001).

electron micro-diffraction suggest that the particles have an amphibole structure, and are probably a hornblende. The distribution of these particles in the deformed samples is heterogeneous. Particle-free regions are always dislocation-free. Wide-area EDS analysis shows no significant difference in composition, especially Fe content, between particle-free and particle-bearing regions. These observations suggest

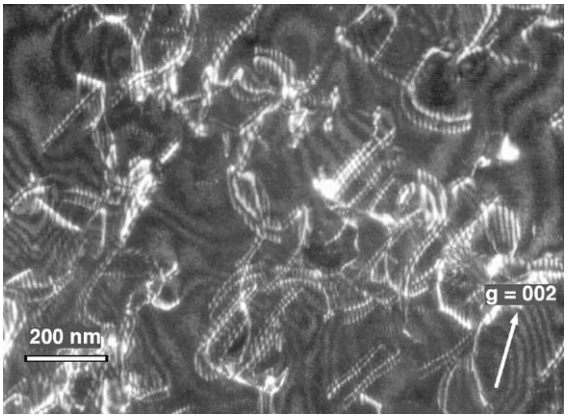


Fig. 7. DF image of region of sample 3 with electron beam near [$\bar{1}\bar{1}$0]. The weakly diffracting conditions (2g/9g) for the 002 reflection reveal many double images of the *b*=[001] dislocations. The linear alignment of many segments, roughly NE–SW, corresponds to screw segments with line directions [001]. Other segments then have mixed character. Almost all of the dislocations here have *b*=[001]. No fault contrast can be seen between the doubled lines. The dotted contrast on each image is characteristic of dislocations inclined in the thin foil.

that the particles have nucleated at dislocations, although there is no indication from dislocation shapes that particles have pinned dislocations.

## 3. Discussion

### 3.1. Slip systems

The observed slip systems and their relative quantitative importance as inferred in this study are compatible with the slip systems in plagioclase determined from other studies of experimentally and naturally deformed samples (Marshall and McLaren, 1977a,b; Olsen and Kohlstedt, 1984, 1985; Montardi and Mainprice, 1987). Usually, two sets of dislocations, sometimes three, with different slip systems can be distinguished in most locations in our samples. In terms of density of dislocations, there is no clear dominance of the [001](010) slip system in sample 3. This observation is somewhat different from those of Olsen and Kohlstedt (1984, 1985), Kruhl (1987a,b), Montardi and Mainprice (1987), Ji et al. (1988), and Ji and Mainprice (1987, 1988, 1990) who have inferred a dominance of the [001](010) slip system in plagioclase based on TEM observations and/or on the commonly observed crystallographic preferred orientation (CPO) pattern of (010) planes subparallel to foliation and [001] parallel to lineation in natural mylonites. This same CPO pattern has also been observed by Jensen and Starkey (1985), Olesen (1987), Ji et al. (1993), and Kruse et al. (2001), and appears to be rather typical for plagioclase-dominated mylonites deformed by crystal plastic mechanisms at amphibolite and granulite facies conditions. The lack of a clear predominance of the [001](010) slip system in sample 3 could be due to the fact that all observed slip systems in that sample have similar Schmid factors (Table 2). Our observations are more like those of Kruse et al. (2001) of a natural mylonite (deformed around 700 °C), which contains porphyroclasts suitably and unsuitably oriented for slip on the [001](010) slip system: the dislocations of the [001](010) and the ⟨110⟩ Burgers vector slip systems are similarly abundant. In the recrystallized parts of mylonites a similar abundance of several types of dislocations has been observed (Kruse and Stünitz, 1999). Thus, analyses of dislocations in both experimental samples of this study and some naturally deformed samples indicate that several slip systems are generally important for the plastic deformation of plagioclase, the most common being [001](010) and ⟨110⟩ with slip plane (001) to {111}. We observe that screw dislocations of all Burgers vectors commonly appear free to slip on a range of planes that are characterized by high resolved shear stresses.

### 3.2. [001] Double images

Olsen and Kohlstedt (1984) and Montardi and Mainprice (1987) previously reported image doubling of dislocations with [001] Burgers vector. The details of separation distances, including differences between screw and edge segments, are essentially the same as we observe. Both pairs of authors interpreted the double image to be due to dislocation dissociation,

$$[001] = 1/2[001] + 1/2[001]. \quad (1)$$

Montardi and Mainprice (1987) noted that fault contrast was weak between the two proposed partial dislocations indicating a small stacking fault vector, so that dissociation into at least one extra unidentified partial had to be invoked to explain the observations. Similar weakness in fault contrast was described in

Section 2.4.5 and is totally inconsistent with the $R = 1/2[001]$ fault vector implied by reaction (1). On the other hand, the image visibility of the dislocation pairs can only be interpreted by a Burgers vector parallel to [001], consistent with reaction (1). The weak fault contrast and the image asymmetry indicate some lattice distortion in the region between each of the 'partial' dislocations. The fringe termination method of Ishida et al. (1980) was employed to identify the magnitude of the Burgers vector for the two 'partials' here, but produced ambiguous results. Consequently, even though this type of image has been interpreted as common dissociation of [001] dislocations, the inconsistencies in image detail reveal that such an interpretation is too simplistic. Consideration needs to be given in any further work to identifying contributions from other processes such as dislocation core delocalization, perhaps associated with local changes in Al–Si ordering state, or chemical unmixing. Any core ordering or unmixing would be expected to significantly limit dislocation motion.

It is clear that all [001] dislocations in the deformed Sonoran plagioclase have a complex structure extended along the (010) plane at the tens of nanometre scale. Perhaps it is this core which dictates that [001] dislocations can move only in the (010) plane, resulting in the observed loops being very planar and each parallel to a single slip plane. This behaviour is in strong contrast to the more complexly shaped dislocations of the other observed Burgers vectors ($\langle 110 \rangle$ and [101]) which are able to move on a range of different slip planes. However, judging from [001] dislocation shapes (rectangular loops with long screw segments), either they are not obviously immobilized by having such wide and complex cores, or the cores extended after the dislocations had moved into their current configurations.

### 3.3. Dislocation generation

Given the dislocation-free nature of the starting material, we conclude that all observed dislocations have been generated during the experimental deformation. Some regions remain dislocation free in all samples and can be recognized even using light microscopy by a lack of undulatory extinction. The plastically deformed regions with dislocations are always associated with fractures and/or deformation bands (probably healed cracks in samples 1 and 2) or with grain boundaries (in our case the sample boundaries). One important way to propagate plastic deformation involves glissile dislocations that spread from the high dislocation density regions of deformation bands and fractures (Fig. 5d,e). The deformation bands can generate different sets of dislocations (Fig. 5e). The same slip systems as those spreading from deformation bands have been identified as free dislocations as well. Sample 3 is pervasively plastically deformed and contains two sets of abundant deformation bands. It is probable that most of the free dislocations in this sample have been generated from the deformation bands. The origin of deformation bands in sample 3 is not clear but their orientation is that of active slip planes. As the deformation bands in samples 1 and 2 for the most part probably represent healed cracks we conclude that most of the dislocation generation necessary for plastic deformation in these analyzed samples is produced during a brittle precursor stage of cracking or microcracking.

The generation of dislocations by fracturing has already been described by McLaren and Pryer (2001) for plagioclase and by FitzGerald et al. (1991), McLaren et al. (1989), and Hirth and Tullis (1994) for quartz. These authors have suggested that in the semi-brittle regime of deformation there is not only a superposition of fracturing and dislocation glide processes but that these processes interact and are mutually interdependent. The microstructures observed in our samples indicate the same situation and suggest a similar interpretation. In samples 1 and 2, the plastic deformation is concentrated in rims adjacent to sample margins (Figs. 3 and 4a,e). It is likely that these margins have contained many microcracks or other defects from sample coring and grinding. The reason for the localization of plastic deformation in these portions of the samples may be that plasticity has been initiated by such defects, analogous to plasticity being related to deformation bands and shear fractures. The fact that [001](010) dislocations are observed in sample 1, where this slip system was macroscopically unstressed, is a further indication that this set of dislocations may be generated at deformation bands and shear fractures. The relationship between fracturing and onset of crystal plastic deformation in plagioclase has also been demonstrated by Tullis et al.

(1990) and Tullis and Yund (1992). The onset of crystal plastic deformation in their experiments occurs in a P,T-regime where distributed fracturing is pervasive in the samples and plastically deformed zones occur between the fractures.

The interdependence of fracturing and crystal plastic deformation observed in the experimental samples has important implications for plagioclase deformation in nature. Naturally deformed feldspars show evidence for fracturing during high temperature deformation, even as high as 700–900 °C, when dislocation creep clearly is the dominant deformation mechanism (e.g. Goode, 1978; Sodre Borges and White, 1980; Brown and Macaudiere, 1984; Kruse and Stünitz, 1999; Kruse et al., 2001). Thus, fracturing almost always accompanies crystal plastic deformation of plagioclase in nature. The fracturing appears to be a common precursor to the generation of dislocations, certainly in the low temperature plasticity regime. In this way, the interaction of fracturing and dislocation activity is likely to promote the transition from brittle to plastic deformation in feldspar. Fracturing in feldspars is especially easy because of their two perfect cleavage systems (Tullis and Yund, 1985, 1987, 1992; Hadizadeh and Tullis, 1992). The interaction of fracturing and dislocation activity is potentially important for other minerals with well developed cleavage systems, such as amphiboles and pyroxenes (Kenkmann and Dresen, 2002). The importance of the described interaction for minerals without prominent cleavage systems, such as quartz, is not obvious but the observations of McLaren et al. (1989), FitzGerald et al. (1991), and Hirth and Tullis (1994) in quartz suggest that a similar interdependence can be expected.

### 3.4. $H_2O$-weakening

There seems to be no pronounced weakening effect from the added $H_2O$ in sample 1. The presence of a fluid under undrained deformation conditions increases the pore fluid pressure and tends to promote fracturing (e.g. Paterson, 1978). However, there is no greater density of fractures nor a greater displacement along observed fractures in the $H_2O$-added sample 1 compared to the as-is sample 2. Sample 1 is stronger than sample 2, so that the amount of fluid (0.1 wt.%) is obviously too small to cause embrittlement through lowered effective normal stress, probably because of the low porosity of single crystal samples.

There seems to be no apparent $H_2O$-weakening effect on the plastic deformation either, because the strengths of the water-added (sample 1) and the as-is sample (sample 2) in the same orientation seem to correlate more with the volume of plastically deformed parts of the sample than on $H_2O$ content (see Section 2.3). The plastically deformed parts are not only concentrated at the ends of the cylinders but occur in rims all around the sample pieces so that deformation clearly is not an end-effect of the sample geometry. Furthermore, no melt residue has been observed in any of the samples so that adding of $H_2O$ has not produced any melt.

One explanation for the apparent absence of $H_2O$ weakening is that volume diffusion of $H_2O$ in feldspar is too slow to cause penetration of $H_2O$ throughout the samples during the course of an experiment. The same effect has been observed by Kronenberg et al. (1986) in experimentally deformed samples of quartz. The penetration of $H_2O$ in quartz was found to be facilitated through cracks produced during sample preparation. A similar source of initial microfractures and cracks from sample preparation is probable in our samples. The plastically deformed rims of samples 1 and 2 have the same thickness (Section 3.4) and probably correspond to the potential penetration depth of $H_2O$ into the samples. The microstructures in the light and transmission electron microscope are very similar in the water-added and as-is samples. Thus, given the similarity of microstructures and unclear difference in mechanical data (strain rate effect due to more rim material in the as-is sample) between the water-added and as-is sample, the question of $H_2O$ weakening remains unresolved in this study. The fact that dislocations moved throughout sample 3 suggests that dislocations of at least three Burgers vectors could nucleate, multiply and glide, even though no water was added to this sample.

### 3.5. Recrystallization

No clear recovery features such as subgrains have been observed in any of our plagioclase samples. This situation is in agreement with the observations by Tullis and Yund (1992) for 900 °C experiments on anorthosite and by McLaren and Pryer (2001) and Ji

and Mainprice (1987) for 800 °C experiments on labradorite and albite. Thus, rotation recrystallization does not occur at strain rates of $7.5-8.7\times10^{-7}$ $s^{-1}$ and temperatures up to 900 °C. However, small, defect-free grains occur in healed crushed zones associated with shear fractures (Fig. 5a,c). The fact that the small grains do not display clast-like, irregular outlines but instead rounded shapes, suggests that their grain boundaries have been mobile and are in their present configuration as the result of grain boundary migration. Small, defect-free grains are expected to grow relative to their high-defect-density neighbours and the non-crushed portion of the single crystal adjacent to the crushed zone because of the difference in dislocation density. Furthermore, the small grain size in fracture zones provides a high surface energy to drive normal grain growth. Thus, such small defect-free fragments may act as nuclei for recrystallization by grain boundary migration.

Similar microstructures have been observed in experimentally deformed albite aggregates and anorthosites by Tullis and Yund (1987, 1992), and recrystallization by grain boundary bulging in initially crushed zones has been demonstrated in experiments by Tullis et al. (1990) and Tullis and Yund (1992). The recrystallization in their samples is facilitated by fracturing and is the prerequisite for dislocation creep deformation in the so-called regime 1 in fine grained feldspar aggregates.

It has been inferred that new grains during the dynamic recrystallization in plagioclase may form by classical nucleation (White, 1975; Marshall and Wilson, 1976). One argument for classical nucleation is derived from the chemical changes that frequently are observed between old and new plagioclase grains (White, 1975; Brown et al., 1980; Sodre Borges and White, 1980; Brodie, 1981; Olsen and Kohlstedt, 1985; Molli, 1994; Stünitz, 1998). However, large numbers of new grains without chemical change and without host–control relationship to parent grains have been observed in experimentally deformed samples (Tullis and Yund, 1985, 1987, 1992; Tullis et al., 1990; Ji and Mainprice, 1987, 1990). The proposed mechanism of nucleation as very small, strain-free fragments resulting from fracturing can explain the observed recrystallization features well. It is unclear to what extent aqueous fluids may enhance this effect.

The nucleation of new grains by crushing and subsequent growth of very small fragments may also explain the non-host control orientation of recrystallized grains observed in naturally deformed plagioclase. In a naturally deformed mylonite, Kruse et al. (2001) have described a non-host control orientation relationship between old and new grains for those porphyroclasts which have developed microfractures during high temperature deformation. Other porphyroclasts well suited for slip on [001](010) (in a "soft" orientation) have no microfractures and show rotation recrystallization and thus a clear host–control relationship between new and old grains. The difference in the orientation relationship can be explained by a difference in the nucleation process for the new grains: fracturing is not likely to produce a host–control orientation relationship and appears to be an effective mechanism for nucleation during recrystallization dominated by local grain boundary processes (bulging) in plagioclase. Recrystallization of plagioclase is dominated by grain boundary bulging in nature and experiments (Tullis and Yund, 1985, 1987, 1992; Tullis et al., 1990; Ji and Mainprice, 1988, 1990; Ji et al., 1988), and the nucleation process through crushing can explain many observations.

The importance of nucleation resulting from crushing for the recrystallization of other minerals is not clear yet. However, the low temperature dynamic recrystallization process in quartz also takes place by grain boundary bulging, producing small new dislocation-free grains in the absence of subgrain formation (Hirth and Tullis, 1992). In naturally deformed quartz, an association between fractures and fine grained recrystallized aggregates at the lowest temperatures of crystal plastic deformation has been observed (van Daalen et al., 1999; Stipp et al., 2002a,b), so that in such cases nucleation of new grains by crushing is likely.

## 4. Conclusions

Deformation experiments on gem quality plagioclase single crystals have been carried out at higher temperatures and slower strain rates (900 °C, $\dot{\varepsilon}=7.5-8.7\times10^{-7}$ $s^{-1}$) than previous experiments and produce semi-brittle to plastic deformation structures,

partly depending on the stress orientation with respect to the crystals. A crystal orientation, denoted "soft", well suited for slip on the [001](010) slip system, is considerably weaker than a "hard" orientation, where the Schmid factor for this slip system is equal to zero. This result confirms that [001](010) is an important slip system in plagioclase as established previously by Marshall and McLaren (1977a,b), Olsen and Kohlstedt (1984, 1985), Montardi and Mainprice (1987), and Ji and Mainprice (1987, 1988, 1990). In our sample in the "soft" orientation, resolved shear stress was also high for other slip systems, and the ⟨110⟩(001) to {111} slip systems are similarly active. A subordinate system with [101] Burgers vector, slipping in $(\bar{1}31)$ to $(\bar{2}42)$, also occurs in the "soft" sample. Dislocations of the [001](010) and the ⟨110⟩(001) to ⟨110⟩{111} slip systems have also been observed in the "hard" sample with zero Schmid factor for [001](010). All dislocations with [001] Burgers vector show a double image with $<50$ nm separation. While simple dissociation can be ruled out to explain this image doubling, further work is needed to fully characterize the dislocation cores.

Fracturing and twinning are mutually dependent processes in the samples in the "hard" orientation, due to stress relaxation around crack tips as described by McLaren and Pryer (2001). The dislocation activity and the resulting portions of crystal plastic deformation are heterogeneously distributed in the sample in the "hard" orientation. Plastic deformation is strongly associated with fractures and deformation bands, which probably represent healed cracks. Glissile dislocations of all observed slip systems spread out from zones of high dislocation density that probably developed during crack healing. Thus, glissile dislocations are generated at or near fractures. The association between twins, dislocations and fractures is very similar to that observed by McLaren and Pryer (2001), who found similar microstructures, although not to the same extent, at lower temperatures of deformation, slightly higher strain rates, and slightly lower finite strains.

$H_2O$ weakening cannot be unequivocally demonstrated in our deformed samples, probably because the potential penetration of $H_2O$ is limited, as in experiments on quartz by Kronenberg et al. (1986). Small particles ($<20$ nm) of amphibole are observed in the plagioclase crystals in association with dislocations indicating that precipitation and nucleation were enhanced by plastic deformation. Subgrain formation has not been observed in any of the samples.

Crushed zones in shear fractures show very small ($<1$ μm), defect-free grains with rounded outlines which have originated as crush zone fragments. These particles appear to act as nuclei for new recrystallized grains. In this way, small grains formed by fracturing may be the sites of nucleation for new grains during grain-boundary-bulging-dominated recrystallization, especially in low-temperature dislocation creep. New grains formed by such a process do not have a host controlled orientation, as also observed in naturally deformed plagioclase. The nucleation of recrystallized grains by small fragments appears to be an important process in the recrystallization of feldspars in experiments and in nature.

## Acknowledgements

Our study has in part been initiated after some comments by David Mainprice and has benefited a lot from many discussions with Dick Yund. The work has been supported by a visiting fellowship from the Research School of Earth Sciences to H.S. during his stay at the Australian National University, by NSF grant EAR 9628348, and by Swiss Nationalfonds projects 2000-63662.01 and 2001-65041.01. The manuscript was greatly improved by the thorough and very constructive reviews by Georg Dresen and Kyu Kanagawa. We thank all of them very much.

## References

Borg, I.Y., Heard, H.C., 1970. Mechanical twinning and slip in experimentally deformed plagioclase. Contrib. Mineral. Petrol. 23, 128–135.

Brodie, K.H., 1981. Variation in amphibole and plagioclase composition with deformation. Tectonophysics 78, 385–402.

Brown, W.L., Macaudiere, J., 1984. Microfracturing in relation to atomic structure of plagioclase from a deformed meta-anorthosite. J. Struct. Geol. 5, 579–586.

Brown, W.L., Macaudière, J., Ohnenstetter, M., 1980. Ductile shear zones in a meta-anorthosite from Harris, Scotland: textural and compositional changes in plagioclase. J. Struct. Geol. 2, 281–287.

Carpenter, M.A.I., 1994. Subsolidus phase relations of the plagio-

clase feldspar solid solution. In: Parsons, I. (Ed.), Feldspars and their Reactions. Kluwer Academic Publishing, Amsterdam, pp. 221–269.

Drury, M.R., Urai, J.L., 1990. Deformation-related recrystallization processes. Tectonophysics 172, 235–253.

FitzGerald, J.D., Boland, J.N., McLaren, A.C., Ord, A., Hobbs, B.E., 1991. Microstructures in water-weakened single crystals of quartz. J. Geophys. Res. 96B, 2139–2155.

Fredrich, J.T., Evans, B., Wong, T.F., 1989. Micromechanisms of the brittle to plastic transition in Carrara marble. J. Geophys. Res. 94B, 4129–4145.

Gleason, G.C., Tullis, J., Heidelbach, F., 1993. The role of dynamic recrystallization in the development of lattice preferred orientations in experimentally deformed quartz aggregates. J. Struct. Geol. 15, 1145–1168.

Goode, A.D.T., 1978. High temperature, high strain rate deformation in the lower crustal Kalka intrusion, Central Australia. Contrib. Mineral. Petrol. 66, 137–148.

Gutmann, J.T., Martin, R.F., 1976. Crystal chemistry, unit cell dimensions, and structural state of labradorite megacrysts from Sonora, Mexico. Schweiz. Mineral. Petrol. Mitt. 56, 55–64.

Hadizadeh, J., Tullis, J., 1992. Cataclastic flow and semi-brittle deformation of anorthosite. J. Struct. Geol. 14, 57–63.

Hirth, G., Tullis, J., 1992. Dislocation creep regimes in quartz aggregates. J. Struct. Geol. 14, 145–159.

Hirth, G., Tullis, J., 1994. The brittle–plastic transition in experimentally deformed quartz aggregates. J. Geophys. Res. 99, 11731–11747.

Hobbs, B.E., 1968. Recrystallization of single crystals of quartz. Tectonophysics 6, 353–401.

Ishida, Y., Ishida, H., Kohra, K., Ichinose, H., 1980. Determination of the Burgers vector of a dislocation by weak-beam imaging in a HVEM. Philos. Mag. A 42, 453–462.

Jensen, L.N., Starkey, J., 1985. Plagioclase microfabrics in a ductile shear zone from the Jotun Nappe, Norway. J. Struct. Geol. 7, 527–539.

Ji, S., Mainprice, D., 1987. Experimental deformation of sintered albite above and below the order–disorder transition. Geodynam. Acta 1, 113–124.

Ji, S., Mainprice, D., 1988. Natural deformation of plagioclase: implication for slip systems and seismic anisotropy. Tectonophysics 147, 145–163.

Ji, S., Mainprice, D., 1990. Recrystallization and fabric development in plagioclase. J. Geol. 98, 65–79.

Ji, S., Mainprice, D., Boudier, F., 1988. Sense of shear in high-temperature movement zones from the fabric asymmetry of plagioclase feldspars. J. Struct. Geol. 10, 73–81.

Ji, S., Salisbury, M.H., Hanmer, S., 1993. Petrofabric, P-wave anisotropy and seismic reflectivity of high grade tectonites. Tectonophysics 222, 195–226.

Kenkmann, T., Dresen, G., 2002. Dislocation microstructure and phase distribution in a lower crustal shear zone—an example from the Ivrea Zone, Italy. Int. J. Earth Sci. 91, 445–458.

Kohlstedt, D.L., Evans, B., Mackwell, S.J., 1995. Strength of the lithosphere: constraints imposed by laboratory experiments. J. Geophys. Res. 100B, 17587–17602.

Kronenberg, A.K., Kirby, S.H., Aines, R.D., Rossman, G.R., 1986. Solubility and diffusional uptake of hydrogen in quartz at high water pressures: implications for hydrolytic weakening. J. Geophys. Res. 91B, 12723–12744.

Kruhl, J., 1987a. Preferred lattice orientations of plagioclase from amphibolite and greenschist facies rocks near the Insubric Line (Western Alps). Tectonophysics 135, 233–242.

Kruhl, J., 1987b. Zur Deformation und Gitterregelung des Plagioklases. Jb. Geol. B.-A. 130, 205–243.

Kruse, R., Stünitz, H., 1999. Deformation mechanisms and phase distribution in mafic high temperature mylonites from the Jotun Complex, Norway. Tectonophysics 303, 223–251.

Kruse, R., Stünitz, H., Kunze, K., 2001. Dynamic recrystallization processes in plagioclase porphyroclasts. J. Struct. Geol. 23, 1781–1802.

Marshall, D.B., McLaren, A.C., 1977a. Deformation mechanisms in experimentally deformed plagioclase feldspars. Phys. Chem. Mineral. 1, 351–370.

Marshall, D.B., McLaren, A.C., 1977b. The direct observation and analysis of dislocations in experimentally deformed plagioclase feldspars. J. Mater. Sci. 12, 893–903.

Marshall, D.B., Wilson, C.J.L., 1976. Recrystallization and peristerite formation in albite. Contrib. Mineral. Petrol. 57, 55–69.

McLaren, A.C., 1991. Transmission Electron Microscopy of Minerals and Rocks. Cambridge Univ. Press, Cambridge. 387 pp.

McLaren, A.C., Pryer, L.L., 2001. Microstructural investigation of the interaction and interdependence of cataclastic and plastic mechanisms in feldspar crystals deformed in the semi-brittle field. Tectonophysics 335, 1–15.

McLaren, A.C., FitzGerald, J.D., Gerretsen, J., 1989. Dislocation nucleation and multiplication in synthetic quartz: relevance to water weakening. Phys. Chem. Mineral. 16, 465–482.

Molli, G., 1994. Microstructural features of high temperature shear zones in gabbros of the Northern Apennine ophiolites. J. Struct. Geol. 16, 1535–1541.

Montardi, Y., Mainprice, D., 1987. A transmission electron microscope study of the natural plastic deformation of calcic plagioclases (An68-70). Bull. Mineral. 110, 1–14.

Olesen, N.O., 1987. Plagioclase fabric development in a high grade shear zone, Jotunheimen, Norway. Tectonophysics 111, 107–131.

Olsen, T.S., Kohlstedt, D.L., 1984. Analysis of dislocations in some naturally deformed plagioclase feldspars. Phys. Chem. Mineral. 11, 153–160.

Olsen, T.S., Kohlstedt, D.L., 1985. Natural deformation and recrystallization of some intermediate plagioclase feldspars. Tectonophysics 111, 107–131.

Paterson, M.S., 1978. Experimental Rock Deformation—The Brittle Field. Springer, Berlin, Heidelberg. 254 pp.

Sodre Borges, F., White, S.H., 1980. Microstructural and chemical studies of sheared anorthosites, Roneval, South Harris. J. Struct. Geol. 2, 273–280.

Stipp, M., Stünitz, H., Heilbronner, R., Schmid, S.M., 2002a. The Eastern Tonale fault zone: a "natural laboratory" for crystal plastic deformation of quartz over a temperature range from 250 to 700 °C. J. Struct. Geol. 24, 1861–1884.

Stipp, M., Stünitz, H., Heilbronner, R., Schmid, S.M., 2002b. Dy-

namic recrystallization of quartz: correlation between natural and experimental deformation conditions. In: de Meer, S., Drury, M.R., de Bresser, J.H.P., Pennock, G.M. (Eds.), Deformation Mechanisms, Rheology and Tectonics: Current Status and Future Perspectives. Special Publication, vol. 200. Geological Society, London, pp. 171–190.

Stünitz, H., 1998. Syndeformational recrystallization: dynamic or compositionally induced? Contrib. Mineral. Petrol. 131, 219–236.

Tullis, J., Yund, R.A., 1985. Dynamic recrystallization of feldspar: a mechanism for ductile shear zone formation. Geology 13, 238–241.

Tullis, J., Yund, R.A., 1987. Transition from cataclastic flow to dislocation creep of feldspar: mechanisms and microstructures. Geology 15, 606–609.

Tullis, J., Yund, R.A., 1992. The brittle–ductile transition in feldspar aggregates: an experimental study. In: Evans, B., Wong, T.F. (Eds.), Fault Mechanics and Transport Properties in Rocks. Academic Press, New York, pp. 89–118.

Tullis, J., Dell'Angelo, L.N., Yund, R.A., 1990. Ductile shear zones from brittle precursors in feldspathic rocks; the possible role of dynamic recrystallization. In: Duba, A., Durham, W., Handin, J., Wang, H. (Eds.), The Brittle–Ductile Transition: The Heard Volume. Am. Geophys. Monograph, Washington, DC, pp. 67–82.

Urai, J.L., Means, W.D., Lister, G.S., 1986. Dynamic recrystallization of minerals. In: Hobbs, B.E., Heard, H.C. (Eds.), Mineral and Rock Deformation: Laboratory Studies. AGU Geophys. Monogr., vol. 36, pp. 161–199.

van Daalen, M., Heilbronner, R., Kunze, K., 1999. Orientation analysis of localized shear deformation in quartz fibres at the brittle–ductile transition. Tectonophysics 303, 83–108.

White, S.H., 1975. Tectonic deformation and recrystallization of oligoclase. Contrib. Mineral. Petrol. 50, 287–304.

Wiederhorn, S.M., 1972. Subcritical crack growth in ceramics. In: Bradt, R.C., Hasselman, D.P.H., Lange, F.F. (Eds.), Mechanics of Ceramics. Plenum, New York, p. 613.

Yund, R.A., Tullis, J., 1991. Compositional changes of minerals associated with dynamic recrystallization. Contrib. Mineral. Petrol. 108, 346–355.